Multichannel Blind Deconvolution of the Short-Exposure Astronomical Images

Filip Šroubek, Jan Flusser, Tomáš Suk
Institute of Information Theory and Automation
Academy of Sciences of the Czech Republic
Pod vodárenskou věží 4, 182 08, Praha 8
{sroubekf, flusser, suk}@utia.cas.cz

Stanislava Šimberová
Astronomical Institue
Academy of Sciences of the Czech Republic
Observatory Ondřejov
ssimbero@asu.cas.cz

Abstract

In this paper we present a new multichannel blind deconvolution method based on so-called subspace technique that was originally proposed by Harikumar and Bresler. When at least two differently degraded images (channels) of the original scene are provided, the method is better conditioned than classical single channel ones. In comparison with earlier multichannel blind deconvolution techniques the subspace method is not iterative and this possibly implies an implementation that can be computationally more efficient. An application of the proposed method to the restoration of the images of sunspots is presented.

1. Introduction

By multichannel (MC) blind deconvolution we understand simultaneous deconvolution of several images obtained by measuring the same scene but convolved with different unknown filters. Since the MC blind deconvolution can often provide much better results than the single channel (SC) approach, that is ill-conditioned and ill-posed, it has found numerous applications in many areas.

The motivation of this work came from solar astrophysics. Pictures taken by a ground-based telescope are often the major information source about the processes on the Sun atmosphere. In the visible spectral band, the effects of the refractive index fluctuation of the air caused by temperature variations become significant. The wavefronts are perturbed and, consequently, the quality of the images decreases. Another limit on image resolution is imposed by an atmospheric turbulence. In a short-exposure image the turbulent medium forms a complex point-spread function (PSF) with a random phase whose mean equals zero for frequencies higher than r_0/λ, where r_0 is a diameter of a diffraction-limited circular pupil that would give an image of the same resolution and λ stands for the wavelength. Knowing the parameters of the telescope we can partially model the PSF. However, due to the random component presented by the atmospheric turbulence a complete modeling of the PSF is impossible. Thus, the image restoration must be viewed as a *blind deconvolution* problem.

In ground-based astronomical observations it is often possible to obtain several images of the object under investigation that differ just by the degradation PSF. A typical example is a short time sequence of pictures of a still scene. Thus, it is possible to use a MC approach to image restoration.

The MC deconvolution problem is in general better conditioned than the SC one when channels with different blur functions are assumed. This problem has recently attracted a considerable attention as new efficient algorithms have been proposed for its solution. First attempts were made in the blind deconvolution of multiple speckle images. SC blind iterative algorithms were applied in parallel here and estimates were averaged [8], [7]. Methods proposed in [1], [2], [10], [11], [6] extend readily available SC blind algorithms to the MC framework. More recently, intrinsically MC blind methods that do not have SC equivalent were proposed, e.g. in [9], [5].

In this paper, we present a new MC blind deconvolution method based on the *subspace technique* that was originally proposed by Harikumar and Bresler [5], [4]. Their work extends the 1-D subspace techniques EVAM [3] to the 2-D scenario. The subspace technique belongs to the set of intrinsically MC blind deconvolution approaches, i.e. it requires at least two differently degraded images of the original scene for a successful restoration. An application of the subspace method to the restoration of the images of sunspots and experiment results are shown in the last section of the paper.

2. Algorithm

We assume the linear shift-invariant degradation that is modeled as

$$\mathbf{Y}_i = \mathbf{X} * \mathbf{H}_i + \mathbf{N}_i, \qquad 1 \le i \le p \tag{1}$$

where $\mathbf{X}$ denotes the discrete original image of size (m_x, n_x) convolved with $p \ge 2$ discrete blur filters $\mathbf{H}_i$ of maximum size (m_h, n_h), $\mathbf{N}_i$ are noise matrices of appropriate size and $\mathbf{Y}_i$ are the observed images. The requirement of *different* measurements corresponds to an assumption that $\mathbf{H}_i$ are coprime, i.e. a scalar constant is the only common factor of the z-transforms $\tilde{H}_i(z_1, z_2)$ of the blurs $\mathbf{H}_i$. It is proved in [5] that in the noise-free case, if $p \ge 2$ and the coprime assumption holds, then all solutions $\mathbf{G}_i$ of size (m_g, n_g) to

$$\mathbf{Y}_i * \mathbf{G}_j - \mathbf{Y}_j * \mathbf{G}_i = \mathbf{0}, \qquad 1 \le i < j \le p \tag{2}$$

have the form $\mathbf{G}_i = \mathbf{H}_i * \mathbf{K}$ for some extra factor $\mathbf{K}$ if $m_g \ge m_h$ and $n_g \ge n_h$. In particular, if $(m_g, n_g) = (m_h, n_h)$, all solutions have the form $\mathbf{G}_i = \alpha \mathbf{H}_i$ for some scalar α. If $m_g < m_h$ or $n_g < n_h$ then (2) has no solution. Using the vector-matrix notation the set of equations (2) can be rewritten as

$$\mathcal{Y}\mathbf{g} = 0 \tag{3}$$

where $\mathbf{g}$ is a vector representation of $[\mathbf{G}_1, \mathbf{G}_2 \ldots \mathbf{G}_p]$. In the presence of noise, however, the situation is different and we look for the least-squares solution to (3) subject to the constraint $\|\mathbf{g}\| = 1$, i.e.

$$\hat{\mathbf{g}}^{(m_g, n_g)} = \arg \min_{\|\mathbf{g}\|=1} \|\mathcal{Y}\mathbf{g}\|^2 \tag{4}$$

where $\hat{\mathbf{g}}$ denotes estimated blurs of size (m_g, n_g) in the vector representation. The dimensions of $\mathcal{Y}$ are very large even for small images. By transferring (3) to the Fourier domain we were able to solve the equation much more effectively without ever having to construct the whole matrix $\mathcal{Y}$ and thus drastically reducing the memory space requirements. Once the estimates $\hat{\mathbf{g}}$ are determined the original image can be restored by standard non-blind deconvolution approaches. Our images contain only a part of the original image and so the *boundary effect* was also considered in our implementation as it is described in [5]. For low SNR (< 30dB) the subspace technique does not give very accurate estimates and an iterative algorithm based on the ML estimates is proposed in [5]. In our case of astronomical images, we certainly know that SNR > 50dB and so the subspace technique gives satisfying results.

The whole restoration procedure of $\mathbf{X}$ was done in four steps:

1. Solve (4) for overestimated size (m_g, n_g), i.e. $m_g > m_h$ and $n_g > n_h$. We know that the solutions have the form $\hat{\mathbf{G}}_i = \mathbf{H}_i * \mathbf{K}$ and thus we may consider the oversized estimates $\hat{\mathbf{G}}_i$ as our new degraded images and apply the subspace technique again. Clearly, this speeds up the whole restoration, because $\hat{\mathbf{G}}_i$ are much smaller than $\mathbf{Y}_i$.
2. Using $\hat{\mathbf{G}}_i$ instead of $\mathbf{Y}_i$ rewrite (4) as $\hat{\mathbf{h}}^{(M_h, N_h)} = \arg\min_{\|\mathbf{e}\|=1} \|\mathcal{G}\mathbf{e}\|^2$ and solve it for all possible supports smaller than (m_g, n_g) to find the blur estimates $\hat{\mathbf{h}}^{(M_h, N_h)}$. In each step the number of unknowns is equal to the blurs support $M_h \times N_h$.
3. For each $\hat{\mathbf{h}}^{(M_h, N_h)}$, the original image estimate $\hat{\mathbf{X}}^{(M_h, N_h)}$ is the one that minimizes the residual $r(\mathbf{Z}) = \sum_i \|\mathbf{Y}_i - \hat{\mathbf{H}}_i * \mathbf{Z}\|^2$. We use the conjugate gradient method to minimize the residuals.
4. $\hat{\mathbf{X}}^{(M_h, N_h)}$ with the *optimal* residual is considered as the best restoration of $\mathbf{X}$. The residual r is not a reliable choice for estimating the proper size (M_h, N_h) because it does not penalize the over-fitting of data and it generally decreases as (M_h, N_h) increases. However, r stays high to a certain breaking point and then it drops down to much smaller values. Estimates $\hat{\mathbf{X}}^{(M_h, N_h)}$ that are just below this edge are regarded as optimal. For estimates of larger (M_h, N_h) strong artifacts, e.g. ringing, tend to show up.

3. Experiment

In this Section, we demonstrate the performance of the proposed method in a real situation. Three images of the spot in the solar photosphere taken by a telescope with a CCD camera are blurred considerably mainly due to the atmospheric turbulence (see Fig. 2). Additive noise is also present but its impact is not significant here. Thanks to high quality of the imaging device, the signal-noise-ratio is higher than 50dB. Since the time interval between each two consecutive acquisitions was very short, the scene can be considered still.

We started with the overestimated blur size $(m_g, n_g) = (20, 20)$, see Section 2 step 1. The estimated blurs $\hat{\mathbf{G}}_i$ where then applied and we solved (4) and minimized the residual 361-times (19×19) as described in the step 2 and 3. Optimal residual was reached for the blur size $(7, 8)$ and the corresponding restored image is in Fig. 2(d). A significant improvement can be seen by visual comparison with the original images. In Fig. 1 one can see another frame from the original observation acquired at the moment when the atmospheric turbulence was very mild. This image was not used in the restoration algorithm. Since it depicted the scene in almost ideal way, it can serve as

image		D
slightly blurred	Fig. 1	10.49
	Fig. 2(a)	4.24
considerably blurred	Fig. 2(b)	5.80
	Fig. 2(c)	4.55
restored	Fig. 2(d)	13.41

Table 1. The measure of the restoration quality D evaluated for blurred images and the restored image.

the reference for evaluation purposes. Visual comparison with the restored image proves a good performance of our restoration technique. As an objective measure of the restoration performance we use an integral of a sum of image partial derivatives

$$D(x) = \int\int \left|\frac{\partial x}{\partial u}\right| + \left|\frac{\partial x}{\partial v}\right| dudv \ , \qquad (5)$$

where x is the image function. If the blur function h is non-negative ($h(u, v) \geq 0$) and it preserves the image energy (i.e. $\int\int h(u, v)dudv = 1$) then $D(x * h) \leq D(x)$. This implies that the value of D increases for less blurred (sharper) images and so it can be used as the measure of the restoration quality. We evaluated integral (5) for images in Figs. 1, 2 and the results are presented in Table 1.

4. Conclusion

We have applied the previously proposed subspace method to the real astronomical data that are of the MC character with a low noise level. In comparison with the original subspace method [5] we have solved the proposed equations in the Fourier domain which dramatically reduces the computation time and memory space requirements and thus enables us to apply this method to large images. We have observed that although the residual is not in theory a reliable choice for estimating the proper size of blurs, i.e. the residual decreases as the blur size increases, a slope of the residual descent can be used as an indication of the proper blur size. We have presented the blurred sunspot images that were used as the input sequence for the subspace method and the final restored image. Apart from the visual comparison that proves a satisfying performance the objective measure of the restoration quality defined as the integral of a sum of image partial derivatives is given.

A majority of MC methods previously proposed reaches estimated solutions by iteratively improving previous estimates. The subspace approach is not iterative in this sense. It estimates PSF of given size in one single step but has to probe different sizes of PSF. Many drawbacks typical for iterative methods, e.g. initial estimates, convergence, local minima, disappear in the subspace approach. On the other hand, the subspace approach gives erroneous results for low signal-noise-ratios compared to iterative methods.

5. Acknowledgment

This work has been supported by the projects No. 102/00/1711 and No. 102/98/PO69 of the Grant Agency of the Czech Republic.

References

[1] K. Boo and N. Bose. Multispectral image restoration with multisensors. *IEEE Trans. Geoscience Remote Sensing*, 35(5):1160–1170, Sept. 1997.

[2] D. Ghiglia. Space-invariant deblurring given N independently blurred images of a common object. *J. Opt. Soc. Am. A*, 1(4):398–402, Apr. 1984.

[3] M. Gurelli and C. Nikias. Evam: An eigenvector-based algorithm for multichannel blind deconvolution of input colored signals. *IEEE Trans. Signal Process.*, 43:134–149, Jan. 1995.

[4] G. Harikumar and Y. Bresler. Efficient algorithms for the blind recovery of images blurred by multiple filters. In *Proceedings of ICIP 96*, volume 3, pages 97–100, Lausanne, Switzerland, 1996.

[5] G. Harikumar and Y. Bresler. Perfect blind restoration of images blurred by multiple filters: Theory and efficient algorithms. *IEEE Trans. Image Processing*, 8(2):202–219, Feb. 1999.

[6] R. Krejčí, J. Flusser, and S. Šimberová. A new multichannel blind deconvolution method and its application to solar images. In *Proceedings of The 14th Internatinal Conf. on Pattern Recognition*, volume 2, pages 1765–1767, 1998.

[7] R. Lane. Blind deconvolution of speckle images. *J. Opt. Soc. Am. A*, 9(9):1508–1514, Sept. 1992.

[8] N. Miura, S. Kuwamura, N. Baba, S. Isobe, and M.Noguchi. Parallel scheme of the iterative blind deconvolution method for stellar object reconstruction. *Applied Optics*, 32(32):6514–6520, Nov. 1993.

[9] S. Pillai and B. Laing. Blind image deconvolution using a robust GCD approach. *IEEE Trans. Image Processing*, 8(2):295–301, Feb. 1999.

[10] A. Rajagopalan and S. Chaudhuri. A recursive algorithm for maximum likelihood-based identification of blur from multiple observations. *IEEE Trans. Image Processing*, 7(7):1075–1079, July 1998.

[11] T. Schulz. Multiframe blind deconvolution of astronomical images. *J. Opt. Soc. Am. A*, 10(5):1064–1073, May 1993.

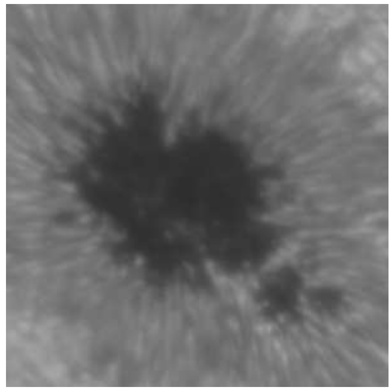

Figure 1. The gray-scale image (300×300) of the sunspot. Due to good atmospheric conditions this observation is negligibly blurred.

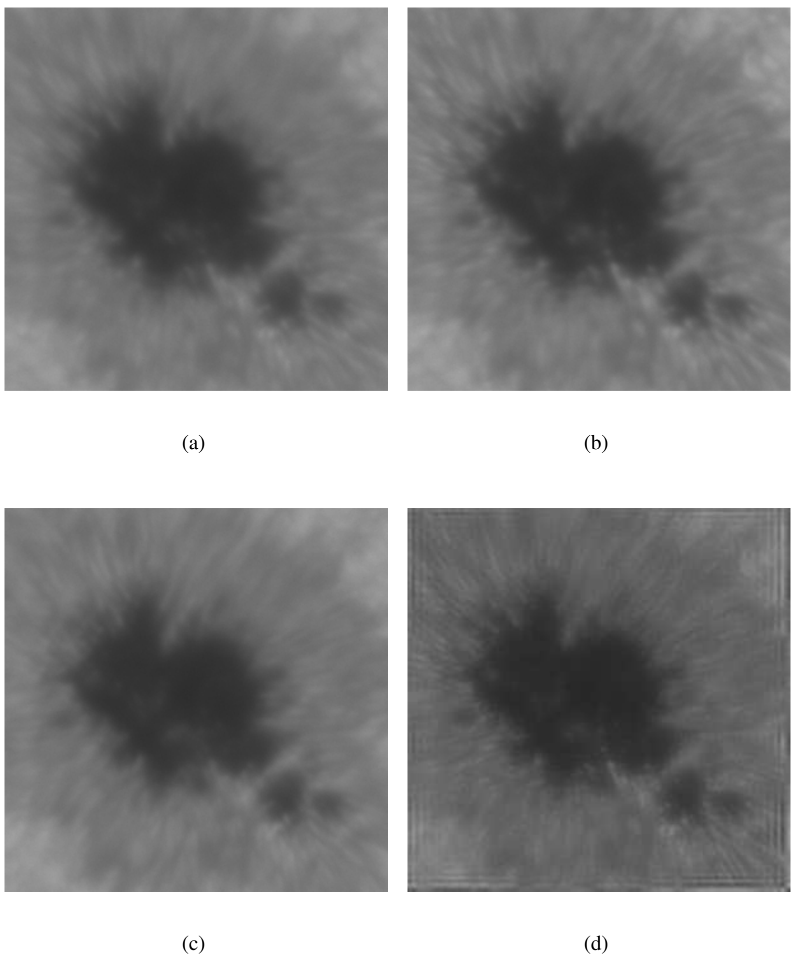

Figure 2. (a)-(c): Other observations of the same sunspot as in Fig. 1. The images are blurred considerably by a varying atmospheric turbulence. (d): The restored image from the sequence (a)-(c) using the proposed subspace technique.